Clim Dyn
DOI 10.1007/s00382-012-1394-0

Teleconnections associated with Northern Hemisphere summer monsoon intraseasonal oscillation

Ja-Yeon Moon · Bin Wang · Kyung-Ja Ha · June-Yi Lee

Received: 1 March 2012 / Accepted: 7 May 2012

Abstract The boreal summer intraseasonal oscillation (BSISO) has strong convective activity centers in Indian (I), Western North Pacific (WNP), and North American (NA) summer monsoon (SM) regions. The present study attempts to reveal BSISO teleconnection patterns associated with these dominant intraseasonal variability centers. During the active phase of ISM, a zonally elongated band of enhanced convection extends from India via the Bay of Bengal and Philippine Sea to tropical central Pacific with suppressed convection over the eastern Pacific near Mexico. The corresponding extratropical circulation anomalies occur along the waveguides generated by the North African-Asian jet and North Atlantic-North European jet. When the tropical convection strengthens over the WNPSM sector, a distinct great circle-like Rossby wave train emanates from the WNP to the western coast of United States (US) with an eastward shift of enhanced meridional circulation. In the active phase of NASM, large anticyclonic anomalies anchor over the western coast of US and eastern Canada and the global teleconnection pattern is similar to that during a break phase of the ISM. Examination of the evolution of the BSISO teleconnection reveals quasi-stationary patterns with preferred centers of teleconnection located at Europe, Russia, central Asia, East Asia, western US, and eastern US and Canada, respectively. Most centers are embedded in the waveguide along the westerly jet stream, but the centers at Europe and Russia occur to the north of the jet-induced waveguide. Eastward propagation of the ISO teleconnection is evident over the Pacific-North America sector. The rainfall anomalies over the elongated band near the monsoon domain over the Indo-western Pacific sector have an opposite tendency with that over the central and southern China, Mexico and southern US, providing a source of intraseasonal predictability to extratropical regions. The BSISO teleconnection along and to the north of the subtropical jet provides a good indication of the surface sir temperature anomalies in the NH extratropics.

Keywords Teleconnection · Intraseasonal variation · Monsoon · Boreal summer intraseasonal oscillation

1 Introduction

Boreal summer intraseasonal oscillation (BSISO) exhibits complex and interactive propagation features (Zhu and Wang 1993; Wang and Rui 1990; Wang and Xie 1997; Annamalai and Slingo 2001), including equatorial eastward propagation (Madden and Julien 1971; Hsu et al. 2004), poleward propagation over the northern Indian Ocean and western North Pacific (Yasunari 1979; Kawamura et al. 1996; Kemball-Cook and Wang 2001; Teng and Wang 2003; Jiang et al. 2004), as well as into the southern hemisphere (Comeaux 1991; Krishnamurti et al. 1992). In addition, there is westward propagation from the western North Pacific to Indian monsoon region on a shorter (10–25 day) time scale (Chen and Murakami 1988; Fukutomi and Yasunari 1999; Annamalai and Slingo 2001; Mao and Chan 2005; Yang et al. 2008; Kikuchi and Wang 2009). A seesaw teleconnection in rainfall anomalies was

J.-Y. Moon · B. Wang · J.-Y. Lee
International Pacific Research Center, School of Ocean and Earth Science Technology, University of Hawaii at Mânoa, Honolulu, HI, USA

K.-J. Ha (✉)
Division of Earth Environmental System, Pusan National University, Busan, Korea
e-mail: kjha@pusan.ac.kr

Published online: 17 August 2012

found between the southern Bay of Bengal (5°–15°N, 80°–100°E) and the eastern Pacific-Mexico (5°–15°N, 85°–105°W) with a quasi-monthly (32 day) time scale (Wang et al. 2006). Through the propagating process, BSISO plays an important role in modulating global scale tropical-extratropical circulation anomalies and severe weather systems such as tropical cyclones (Kikuchi and Wang 2010). It is also a possible source of seasonal climate predictability for precipitation (Wang et al. 2009; Lee et al. 2010) and extratropical atmospheric circulation (Lee et al. 2011).

The features of BSISO and its association with the Asian and North American summer monsoon have been extensively documented by the previous studies (Knutson et al. 1986; Kawamura et al. 1996; Mo 2000; Higgins et al. 2000; Annamalai and Slingo 2001; Lorenz and Hartmann 2006; Ding and Wang 2007; Jiang and Lau 2008; Jiang and Waliser 2009). As the BSISO convection activates over the western North Pacific, distinct trans-Pacific wave train extends to eastern Pacific/North America along a "great circle" route and influences the North American monsoon with somewhat shorter time scale of 20–28 days (Mullen et al. 1998; Mo 2000; Jiang and Lau 2008). Ding and Wang (2007) found a coupled intraseasonal mode between the northern Indian summer monsoon and mid-latitude circulation, which involves an eastward and southward propagation of the wave train originating from the northeastern Atlantic that affects the intraseasonal variability in the northwestern India and Pakistan; meanwhile the rainfall variation over Northern Indian monsoon region can reinforce downstream propagation of wave trains in the mid-latitude.

When the BSISO convection is enhanced over the entire Asian summer monsoon trough (consistent with the active cycle of the Asian summer monsoon), stretching from the Indian continent through the Bay of Bengal, South China Sea to the equatorial west Pacific, the large scale meridional circulation and Walker-type east–west circulations that cover most of the tropics are significantly enhanced (Annamalai and Slingo 2001), which must have an immense impact on the extratropical circulation through excitation and propagation of Rossby wave trains. However, description of BSISO teleconnection pattern from a global perspective has not been systematically investigated and our knowledge on the temporal and spatial structures and dynamics of BSISO teleconnection is still limited. In addition, it is important to examine the evolutionary features of the teleconnection when the BSISO progress from one to another phase.

The objective of the present study is to document global scale BSISO teleconnection and its evolution characteristics. In Sect. 2, the data and statistical method used in this study are described. The dominant modes of BSISO and its connection with the extratropical circulation anomalies are documented in Sect. 3. Time evolutions of the BSISO teleconnection according to each monsoon indices are explored in Sect. 4. The BSISO teleconnection and its impact on the precipitation and temperature distributions over the NH are described in Sect. 5. Conclusion is given in Sect. 6.

2 Data and methodology

The data used in the present study include daily data derived from the ECMWF ERA-Interim reanalysis and Advanced Very High Resolution Radiometer (AVHRR) daily mean outgoing longwave radiation (OLR) from 1979 to 2010. Daily precipitation data over land area (1979–2005) from Climate Prediction Center (CPC) unified global gauge daily analysis (Xie et al. 2007) are also used to investigate the influence of the extratropical teleconnection patterns on precipitation over the NH land areas. Boreal summer is defined as June through September (JJAS).

The BSISO is known to have two major peaks, roughly 30–60 day and 10–25 day. The shorter time scale (10–25 day) convection and its associated extratropical circulation is found to have rather regional scale phenomena (Annamalai and Slingo 2001; Yang et al. 2008). The present study will focus on global perspective of BSISO which has a peak in 30–60 day range. The Lanczos band-pass filter (Duchon 1979) with a cut off period of 30–60 day is applied to daily datasets.

A Student's t test was used to assess the statistical significance of the regression analysis in Sects. 3 through 5.

To reveal energy propagation along the wave train in the extratropics, the wave activity flux vector (Plumb 1985) is analyzed in Sect. 4. The 2-D wave activity flux in relation to Rossby wave train pattern is calculated in spherical coordinates as follows.

$$\textit{Wave activity flux}(WAF) = \frac{\mathrm{p}\cos\emptyset}{\mathrm{p}_0} \times \left\{ \begin{array}{c} \mathrm{v}'^2 - \frac{1}{2\Omega \mathrm{a}\sin\phi}\frac{\partial(\mathrm{v}'\Phi')}{\partial\lambda} \\ -\mathrm{u}'\mathrm{v}' + \frac{1}{2\Omega \mathrm{a}\sin\phi}\frac{\partial(\mathrm{u}'\Phi')}{\partial\lambda} \end{array} \right\} \quad (1)$$

where ($\varnothing$, λ) are the (latitude, longitude); p is pressure; $\mathrm{p}_0 = 1{,}000$ mb; u′, v′, and Φ are the stationary disturbance's zonal wind, meridional wind, and geopotential height, respectively; a and Ω are the earth's radius and rotation frequency, respectively. The WAF provides direct information on wave activity propagation, as the flux is parallel to the group velocity of Rossby waves.

3 Dominant modes of the BSISO teleconnection

In this section, we investigate the teleconnection of the intraseasonal oscillation in the NH summer from three dominant ISO activity centers. During boreal summer, there are three major BSISO convective action centers in the tropics which are also associated with the active/break cycles of boreal summer monsoons. Figure 1 shows that large ISO variances are found in the off-equatorial monsoon troughs over the Indian subcontinent and adjacent ocean, the western North Pacific, and the eastern Pacific near Mexico where Indian (I), western North Pacific (WNP), and North American (NA) summer monsoon (SM) prevail, respectively. In the Indian Ocean, two maximum latitude centers are found over the Arabian Sea/Bay of Bengal (10°–20°N) and the equatorial Indian Ocean, respectively, while in the western Pacific and eastern Pacific near Mexico, the centers are concentrated in 10°–20°N latitude bands. The ISO over three locations indicate the active/break ISM, WNPSM, and NASM activity, respectively. Here we select these three intraseasonal action centers to examine the dominant coupled modes between BSISO and the Northern Hemisphere (NH) extratropics.

To objectively find the robust intraseasonal coupled modes between the tropics and the extratropics, we used circulation (dynamic) indices for the ISM, WNPSM, and NASM (Fig. 1). The circulation ISO index (I) for the ISM, WNPSM, and NASM regions are defined using the meridional difference of 30–60 day 850 hPa zonal winds between a southern (or southwestern) and a northern box with respect to each convective maximum variability centers (Wang and Fan 1999; Wang et al. 2001). These meridional shears of zonal winds represent the relative vorticity at the 850 hPa, which measure the strength of the corresponding monsoon trough. The intraseasonal variations of the circulation indices fully represent the active/break cycles of the corresponding summer monsoons.

$$\begin{aligned}\mathrm{ISMI} &= \mathrm{U850}[5^\circ - 15^\circ\mathrm{N},\ 40^\circ - 80^\circ\mathrm{E}] \\ &\quad - \mathrm{U850}[20^\circ - 30^\circ\mathrm{N},\ 70^\circ - 90^\circ\mathrm{E}], \\ \mathrm{WNPSMI} &= \mathrm{U850}[5^\circ - 15^\circ\mathrm{N},\ 100^\circ - 130^\circ\mathrm{E}] \\ &\quad - \mathrm{U850}[20^\circ - 30^\circ\mathrm{N},\ 110^\circ - 140^\circ\mathrm{E}], \\ \mathrm{NASMI} &= \mathrm{U850}[10^\circ - 20^\circ\mathrm{N},\ 140^\circ - 110^\circ\mathrm{W}] \\ &\quad - \mathrm{U850}[20^\circ - 30^\circ\mathrm{N},\ 115^\circ - 90^\circ\mathrm{W}].\end{aligned}$$

To confirm the reliability of the circulation index, we also used convective index as defined by the area-averaged OLR anomalies of each convective maximum variability center (box in dashed line).

$$\begin{aligned}\mathrm{C\_ISMI} &= \mathrm{OLR}[7.5^\circ - 22.5^\circ\mathrm{N},\ 60^\circ - 90^\circ\mathrm{E}], \\ \mathrm{C\_WNPSMI} &= \mathrm{OLR}[10^\circ - 22.5^\circ\mathrm{N},\ 110^\circ - 140^\circ\mathrm{E}], \\ \mathrm{C\_NASMI} &= \mathrm{OLR}[10^\circ - 20^\circ\mathrm{N},\ 120^\circ - 90^\circ\mathrm{W}].\end{aligned}$$

In Sects. 3 and 4, we applied each index to obtain the regressed fields of OLR, 200 hPa geopotential height (GPH200), 850 hPa geopotential height (GPH850), precipitation, and 2 m air temperature (T2m) during NH summer for the period of 1979–2010 (1979–2005 for precipitation).

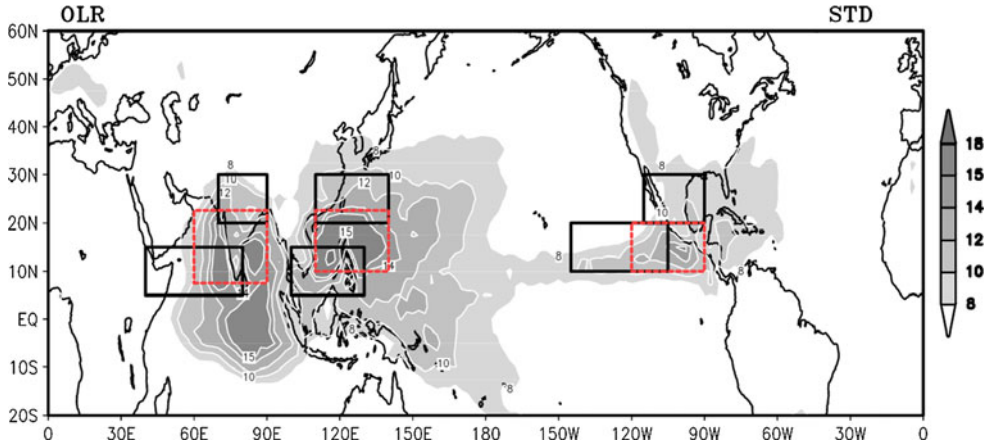

Fig. 1 Standard deviation of the intraseasonal outgoing longwave radiation (OLR) anomaly during the boreal summer (June–September) from 1979 to 2010. The intraseasonal anomaly is defined as the daily data with the long-term mean removed and 30–60 day filtered using Lanczos band-pass filter. *Black solid boxes* indicate the location selected for each circulation monsoon indices: Indian summer monsoon, ISM, U850 (5°–15°N, 40°–80°E: 20°–30°N, 70°–90°E) Western North Pacific summer monsoon, WNPSM, U850 (5°–15°N, 100°–130°E: 20°–30°N, 110°–140°E) and North American summer monsoon, NASM U850 (10°–20°N, 140°–110°W: 20°–30°N, 115°W–90°W). *Red dashed boxes* indicate the location selected for each convective monsoon indices: C_ISM, OLR [7.5°–22.5°N, 60°–90°E], C_WNPSMI = OLR [10°–22.5°N, 110°–140°E], C_NASMI = OLR [10°–20°N, 120°–90°W]. The unit of OLR is W/m^2

3.1 Intraseasonal monsoon indices

We first show the time series of intraseasonal monsoon variability by circulation and convective indices in Fig. 2. The years randomly picked show distinct interannual variability in its amplitude and phase propagation. Both the intraseasonal variability of the circulation and convective indices show similar features such as having the predominant 30–60 day signal, 1979 has the largest amplitude in the early summer. Also, the ISMI and WNPSMI have close time-lagged relationship and the ISMI and NASMI have an opposite tendency. The circulation (convection) index showed ISMI leading WNPSMI by 4–6 (9–10) day with the correlation coefficient 0.5 (0.3), the ISMI and NASMI has the simultaneous (ISMI 1–3 day lead NASMI) correlation of −0.6 (−0.4). There exist some time lag between the circulation and convective indices and the correlation between two different monsoon regions has higher values in circulation indices.

3.2 Regressed teleconnection patterns with respect to three action centers

3.2.1 Circulation indices

To search for the teleconnection patterns associated with the active intraseasonal action centers, we obtained regressed maps of OLR and GPH200 fields with respect to three intraseasonal monsoon circulation indices in Fig. 3. The intraseasonal OLR anomalies associated with the ISMI (Fig. 3a) show a zonally elongated band of active convection from the Arabian Sea via India, Bay of Bengal, and South China Sea, to the Philippine Sea with light convection extending further east to the central Pacific. In the tropics, the zonal extent of the convective activity covers entire tropical Indo-Pacific sector except for the eastern Pacific near Mexico. The suppressed convection is confined to the equatorial eastern Indian Ocean and the eastern Pacific near Mexico. The enhanced convection over Indian subcontinent reflects the active phase of Indian summer

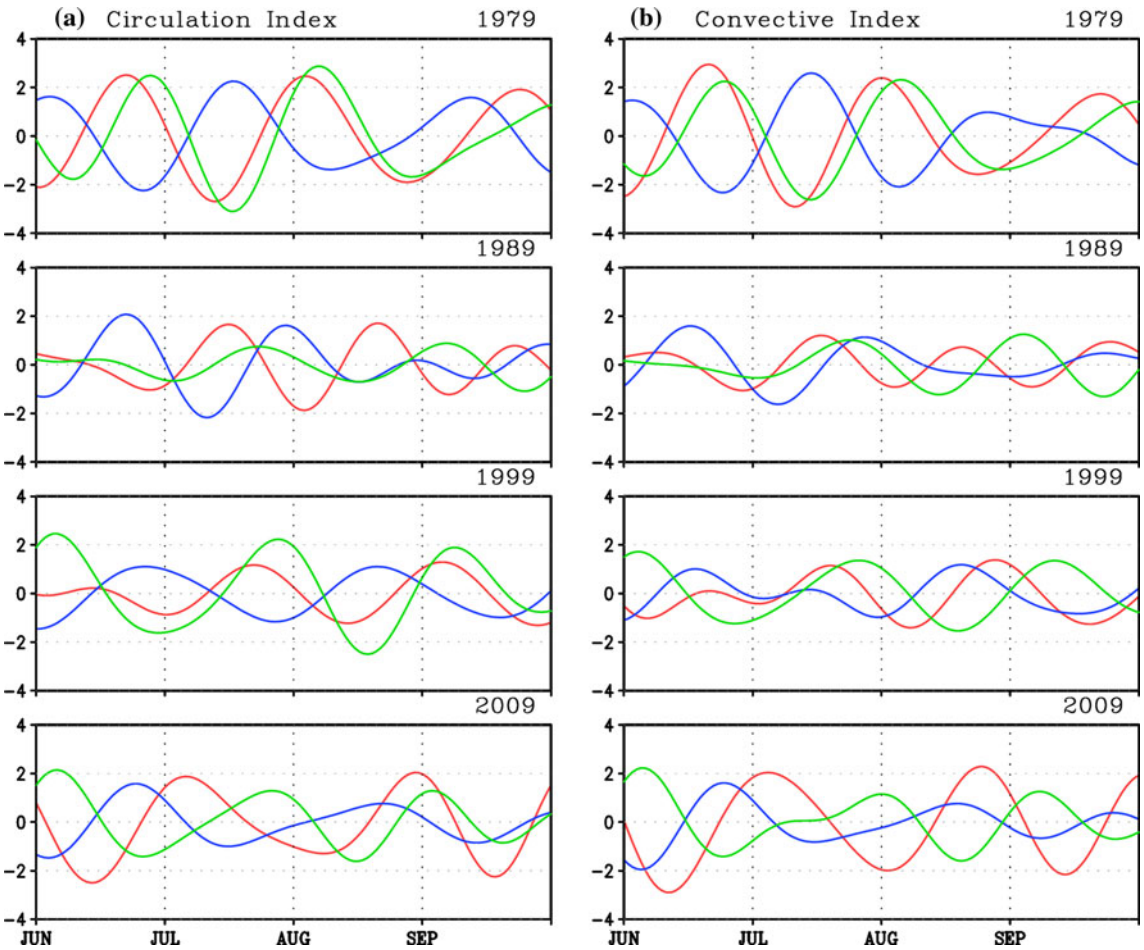

Fig. 2 Intraseasonal monsoon indices by **a** circulation and **b** convection defined based on Fig. 1. Each year is from June 1st to September 30th. Each index is normalized by its standard deviation. *Red*, *green*, *blue lines* indicate ISMI, WNPSMI, NASMI, respectively

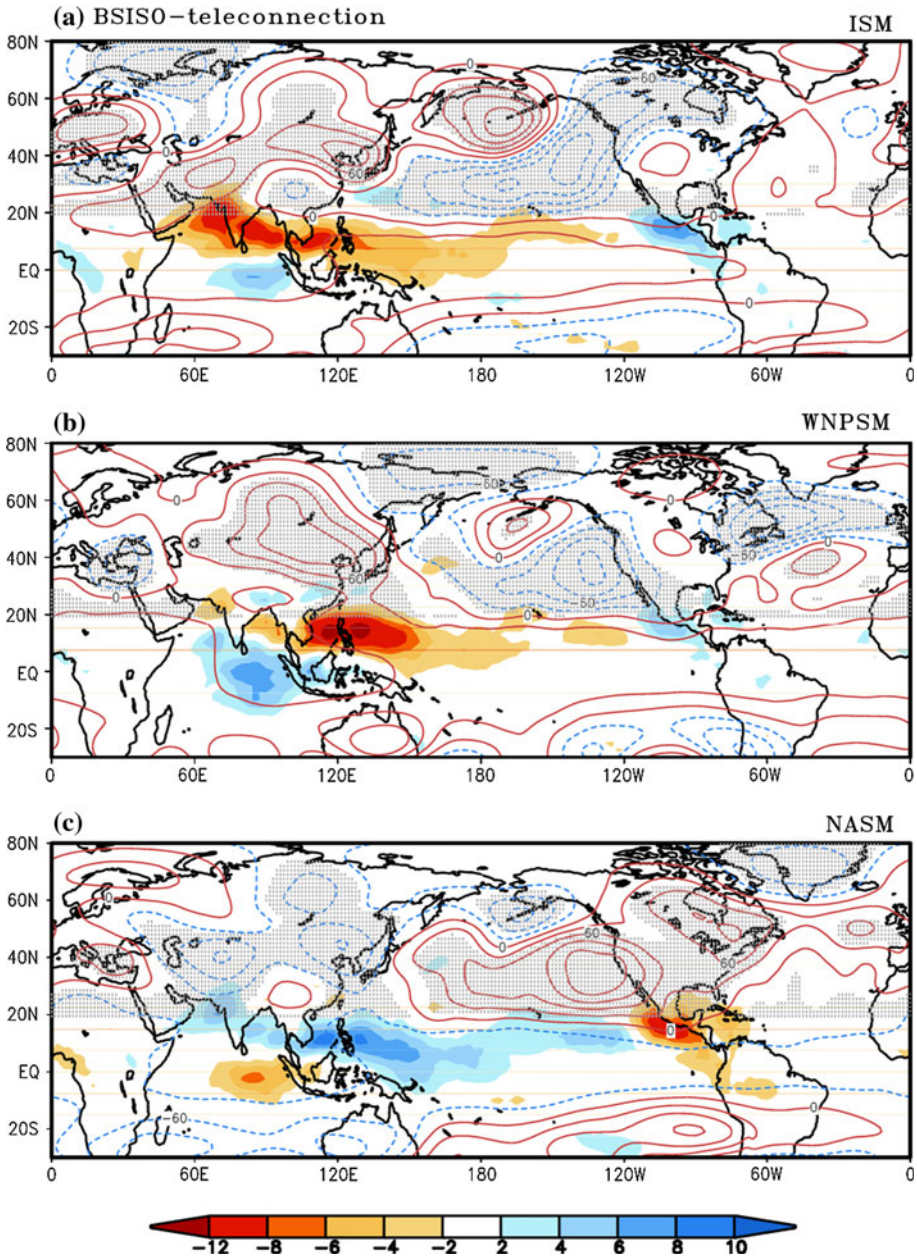

Fig. 3 The regressed intraseasonal anomalies of OLR (*shaded*, in W/m^2) and GPH200 (*contour*, in gpm) against **a** ISM, **b** WNPSM, and **c** NASM circulation indices defined in Fig. 1. *Dotted areas* represent statistically significant regions of GPH200 at 95 % confidence level to the north of 20°N by student's *t* test

monsoon. The extratropical teleconnection pattern associated with this tropical convective activity shows a chain of anomalous anticyclonic centers located at northwest India, East Asia, Aleutian islands in the North Pacific and cyclonic anomalies extends from Southeast Asia through subtropical Pacific-western coast of United States to Canada. In the high-latitudes, a wave-like pattern is also seen from Western Europe to central Siberia. The extratropical wave train over Eurasian sector has been mentioned in Ding and Wang (2007)'s study, which showed the coupled intraseasonal variation with the summer monsoon convection over the northwestern India/Pakistan. Their time-lagged singular vector decomposition analysis showed that the mid-latitude Eurasian wave train originates from the northeastern Atlantic and traverses Europe to central Asia. This equatorward wave train enhances the upper-level high pressure and reinforces the convection over the northwestern India/Pakistan region, which reenergizes the downstream propagation of the wave train to East Asia.

The convective activity associated with the WNPSMI in Fig. 3b shows the largest intensity in the South China Sea-Philippine Sea with a suppressed signal over the equatorial Indian Ocean and eastern Pacific near Mexico. The corresponding GPH200 pattern shows a strong anomalous high over North Asia to the north of the enhanced convection from the WNP and the centers of the negative anomalies positioned over the western and northeastern coasts of North America. Compared to Fig. 3a, the ISO convection

over the northern Indian Ocean has decayed which is related with the weakening of the anticyclonic anomaly over the Southwest Asia while it is more strengthened in the North Asia. The anomalies over the subtropical and North Pacific have weakened with the eastward shift while that over the Atlantic sector shows the intensified feature.

Figure 3c reflects the tropical convection and extratropical circulation anomalies associated with enhanced NASM. The strongest negative anomaly of intraseasonal convection appears over the Mexico and the Gulf of Mexico-Caribbean Sea. The convective activity in Fig. 3c has spatial resemblance with both Fig. 3a, b, but more close to Fig. 3a with the corresponding signs reversed. Figure 3c reveals that the upper-level intraseasonal circulation anomalies associated with an enhanced NASM are an elongated anomalous high stretching from the North Pacific through western coast of United States (US) to Canada and a huge negative anomaly in the Asian continent. Due to the heating from the eastern Pacific near Mexico, the anticyclonic circulation anomaly center near the western coast of US is strong.

From Fig. 3c, the seesaw teleconnection in rainfall anomalies between the southern Bay of Bengal and the eastern Pacific (Wang et al. 2006) is found to be consistent with the convective activity in the present study, indicating that there exist a strong negative phase relationship between the ISMI and NASMI (correlation coefficient is −0.62). Furthermore, the upper-level height anomalies also show a seesaw teleconnection between the Asian continent and North Pacific, which link to opposite convective anomalies between the Indo-west Pacific and eastern Pacific-Mexico, and represent a coherent tropical-extratropical teleconnection.

3.2.2 Convective indices

To compare with the circulation indices, we show in Fig. 4, the regressed OLR and GPH200 with respect to the convective indices. A close look at each regressed OLR patterns show similarities with Fig. 3 in their distribution over the global tropics and the maximum convective centers at each monsoon phases. Meanwhile, there is a slight difference in the location of the convective anomaly especially in ISMI and NASMI. The OLR anomaly in Fig. 4a have maximum center at the northern Bay of Bengal through northern Arabian Sea which is located slightly to the south of that by circulation index. Hence, the circulation/convective index reflect the active convection more towards the northern/southern Indian subcontinent. The convective (suppressed) anomaly over the tropical western-central Pacific (eastern Pacific near Mexico) is weaker compared to Fig. 3a.

Due to the difference of the tropical convective activity, the regressed GPH200 in Fig. 4a also shows a little discrepancy over the Russia-East Asia sector. The southward shift and weakening of the convective activity over the western Pacific is related to the strengthening of the Atlantic-Europe wavetrain and the weakening of the anticyclonic anomaly over the East Asia. In Fig. 4c, the elongated anticyclonic anomaly in the North Pacific-US is shift to west compared to Fig. 3c. From Figs. 3 and 4, it is plausible that there is a little time lag between these two indices. The lead-lag time correlation between the convective and circulation indices for ISMI, WNPSMI, NASMI revealed that the convective index leads circulation index by 2, 0, 3 day with the coefficient of −0.81, −0.88, −0.82, respectively.

Results presented in Figs. 2, 3, 4 basically confirm that the circulation and convective index both can reflect robust and significant BSISO teleconnection by each monsoon indices with time lag. However, for the further analysis, we will focus on the circulation index which showed higher correlation between each monsoon indices (Fig. 1) and also may be more beneficial for the future study that will analyze possible interdecadal variation while the convective index has been limited to the period after 1979.

3.3 Leading modes of BSISO and its teleconnection

To figure out whether the BSISO teleconnection by three intraseasonal monsoon activity centers are the true dominant modes of ISO and ISO teleconnection in the NH summer, we obtained first two leading modes from EOF analysis using 30–60 day filtered OLR anomalies from 1979 to 2010. Figure 5 indicates that the first mode resembles the regressed OLR and GPH200 by WNPSMI and the second mode matches that by ISMI (-NASMI), which proves that three action centers represent resolute dominant modes of BSISO and their teleconnection.

4 Time evolution of the BSISO teleconnection

It is very important to show temporal evolution of the BSISO teleconnection in order to explain the possible cause and effect of the tropical-extratropical interaction. Thus, we obtained regressed OLR and the upper and lower-level geopotential height anomalies against the ISM, WNPSM, and NASM indices at a time lag ranging from −10 to +10 days. To examine the quasi-stationary wave energy propagation, we also diagnose wave activity flux to analyze the global picture of wave propagation along the jet with the evolution of the ISO. The temporal evolution of OLR represents the active cycle of intraseasonal oscillation corresponding to ISM, WNPSM, and NASM, respectively.

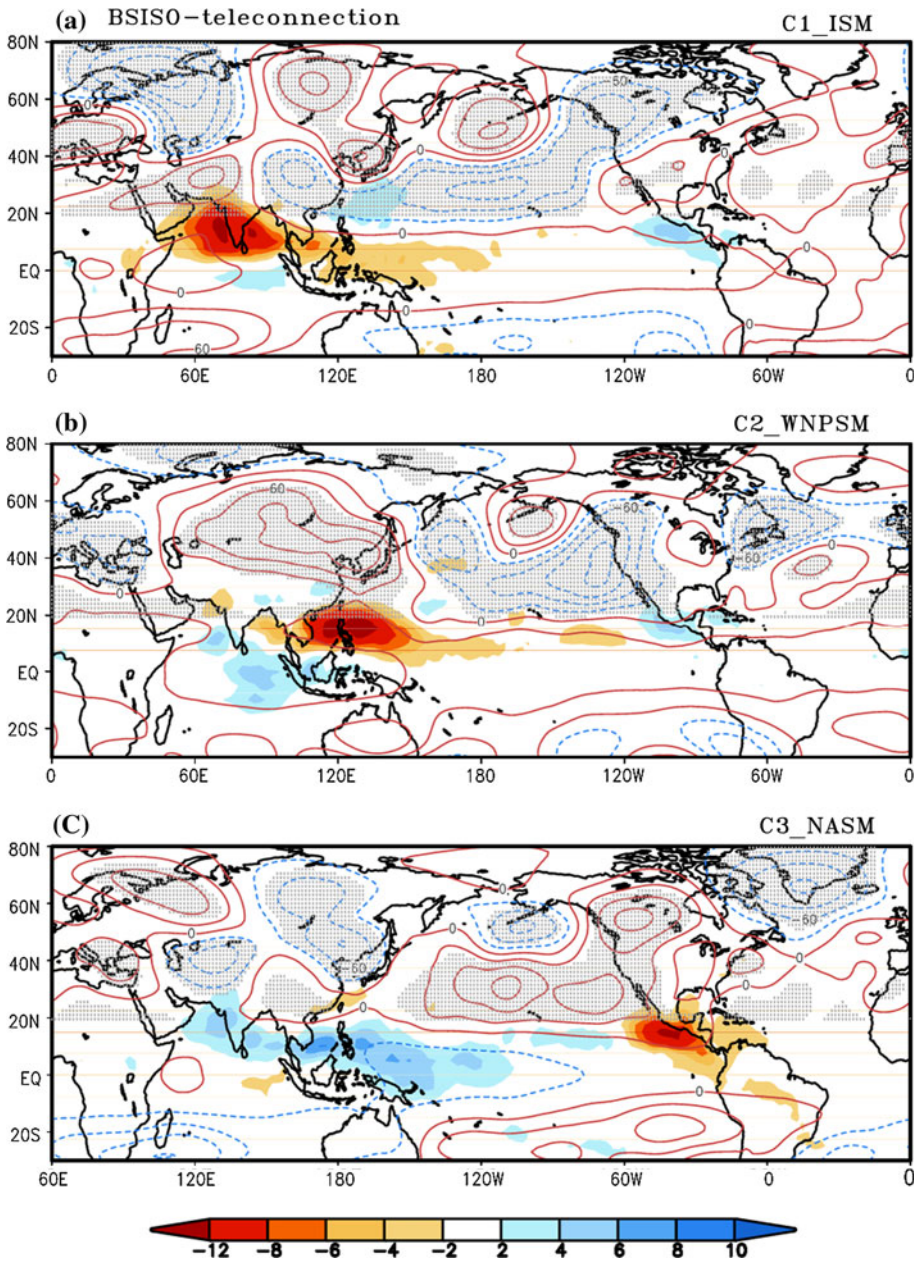

Fig. 4 The regressed intraseasonal anomalies of OLR (*shaded*, in W/m^2) and GPH200 (*contour*, in gpm) against **a** ISM, **b** WNPSM, and **c** NASM convective indices defined in Fig. 1. *Dotted areas* represent statistically significant regions of GPH200 at 95 % confidence level to the north of 20°N by student's *t* test

4.1 The wave trains associated with the ISO over the ISM

Figure 6a displays temporal evolution of the teleconnection pattern associated with ISM ISO. We plotted thickness (GPH200-GPH850) in order to highlight the vertical distance of the teleconnection not only in the extratropics but also near the tropics. At day −10, the ISO convective activity prevails over the region from northern Indian Ocean to maritime continent, while suppressed convection is in the northern side of the convection and over the eastern Pacific near Mexico. At day −5, the negative OLR anomaly intensify and moves north/northwestward and eastward, forming a tilted band structure extending to the central–eastern Pacific. At day 0, negative OLR anomaly over the northern India/Pakistan reaches its maximum and a positive OLR anomaly emerges in the equatorial Indian Ocean, initiating a break cycle of ISM. From day +5, the convective activity further moves northward and eastward at the same time, then weakens at day +10.

Corresponding to the tropical ISO evolution, the circulation (thickness) anomalies at day −10 form a great-circle like wave train from the western coast of US across Atlantic Ocean to western Europe. The path of the wave activity flux also follows the arch-shaped pattern over this sector. From western Europe where the Atlantic jet exit and African jet entrance locates, the wave train splits into two parts; one going northeast to northern Eurasia at the

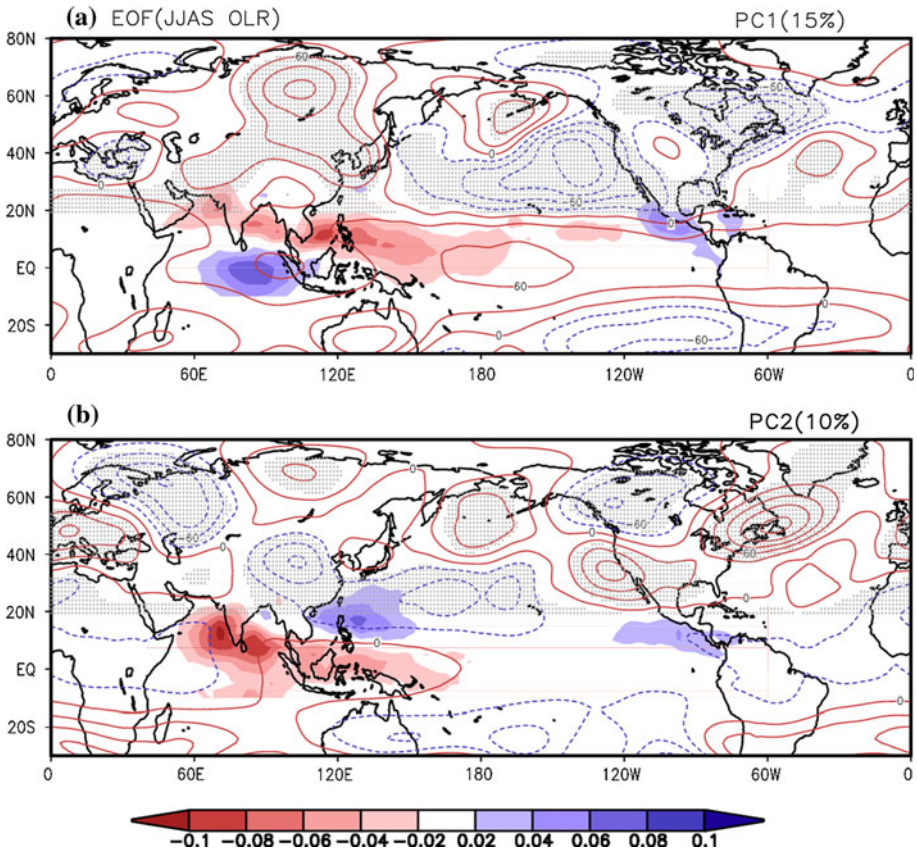

Fig. 5 First two dominant modes from EOF analysis using June–September OLR (*shading*) and regressed geopotential height at 200 hPa by the time coefficient of each eigenvector during 1979–2010. *Dotted areas* represent statistically significant regions at 95 % confidence level to the north of 20°N

north of the jet and the other propagates in southeastward direction to central Asia along the jet. At day −5, the wave energy at the exit of the Atlantic jet strengthens and further transfers energy northeastward to northern Eurasia and southeastward to northern India/Pakistan region. As it was mentioned in Ding and Wang (2007), the anticyclonic anomaly over the northern India/Pakistan region enhances convection and reinforces the Rossby wave train farther downstream along the jet to East Asia. This corresponds well with the direction of the wave activity flux from day −5 to 0. The signal over Europe to Russia in the high latitude slightly weakens at day 0, while the tripolar anticyclonic centers over the central Asia-central Russia-East Asia and the north–south tripole from the tropics to North Pacific are amplified. The cyclonic anomaly over the subtropical North Pacific is induced by the suppressed convection to the north of the active convection over the tropical western/central Pacific and could enhance anticyclonic anomaly to the northern side of the North Pacific. The anticyclonic center over Russia evolves southward and merges at central China where the jet maximum locates from day +5 and the meridional tripole over the Pacific propagates eastward followed by the subsequent propagation of the wave train further downstream to North Atlantic along the jet. At day +10, the wave train from western coast of US transfers energy to downstream region to the exit of the Atlantic jet and starts an opposite signal of day −10.

4.2 The wave train associated with the WNPSM ISO

In Fig. 6b, when the WNPSM is in an active phase, the negative anomaly in the western Pacific is more enhanced while that over the northern Indian Ocean/subcontinent is weakened compared to Fig. 6a. It is clearly seen that the convective activity over the WNP evolves north and northwestward with its intensity amplifies till day 0 and decays as moving further northwestward.

The circulation anomalies regressed against the WNPSMI show similar spatial structures with the ISMI, however, there are several distinct differences. First, the southeastward wave split from the Atlantic jet is weak, which leads to the weakening of convective activity over the northern India/Pakistan region. It is also obvious that the downstream enhancement of the Rossby wave train to East Asia has disappeared compared to Fig. 6a at day −5. Second, the anticyclonic anomaly over the central Russia has the largest amplitude with southward propagation with time and merges with the subtropical anticyclonic center originated from the WNP. Third, the strengthening of the convection over the WNP has induced arch-shaped wave train from the WNP to western coast of US (day +5),

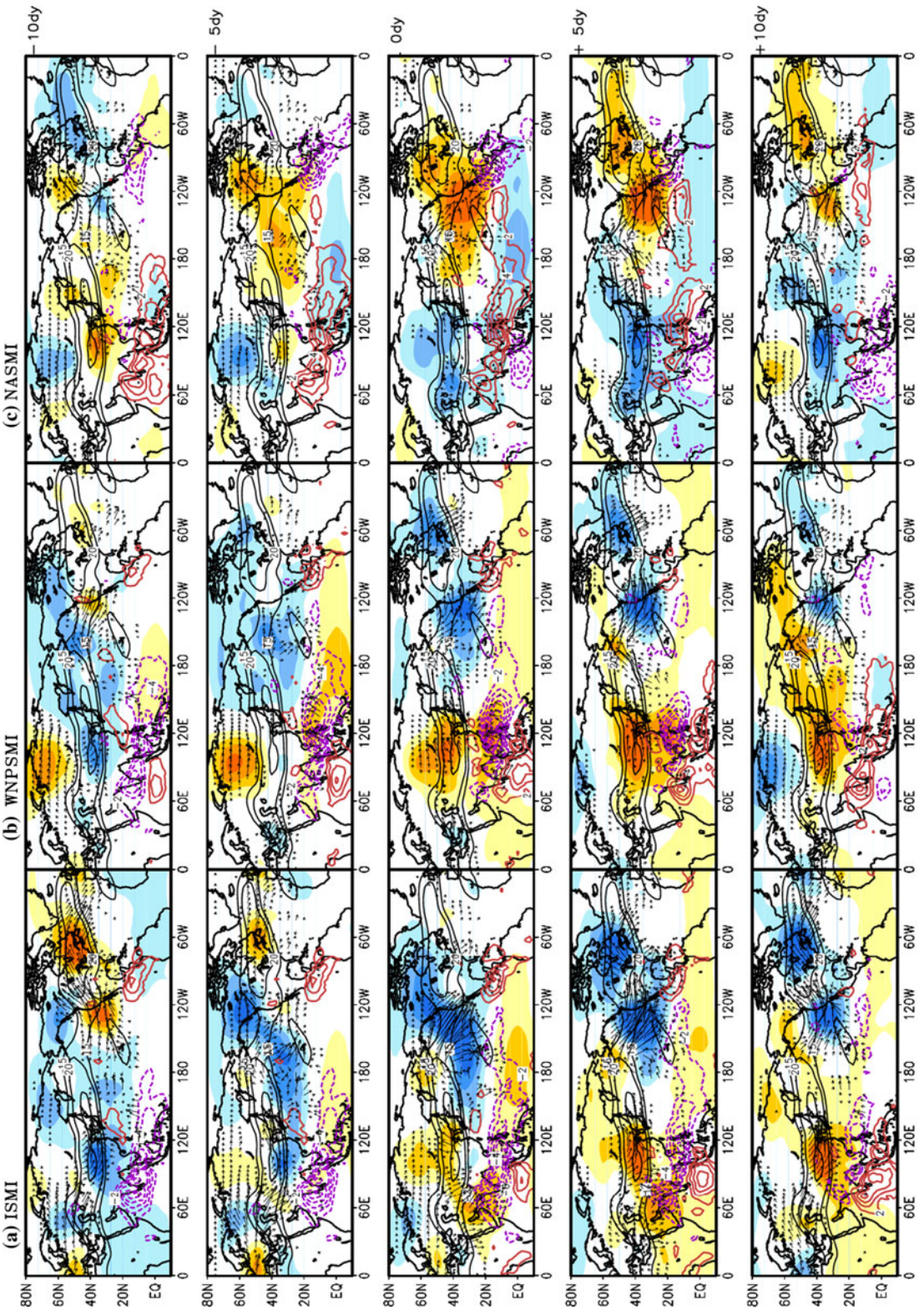

Fig. 6 The lead-lag regression maps of intraseasonal anomalies of OLR (*contour*, negative anomaly depicts active convection, unit: W/m^2), GPH200-GPH850 (*shading*, unit: gpm), and the wave activity flux (vector) with reference to **a** ISM, **b** WNPSM, and **c** NASM indices from −10 to +10 day with a 5-day time interval. The seasonal (June–September) mean westerly (*thick contour* above 15 m/s) wind is plotted to analyze how the wave energy moves along the subtropical jet. Statistically significant regions at 95 % confidence level are *shaded*. Wave vectors with both components less than 0.1 × 10^6 m^2 s^{-1} is omitted

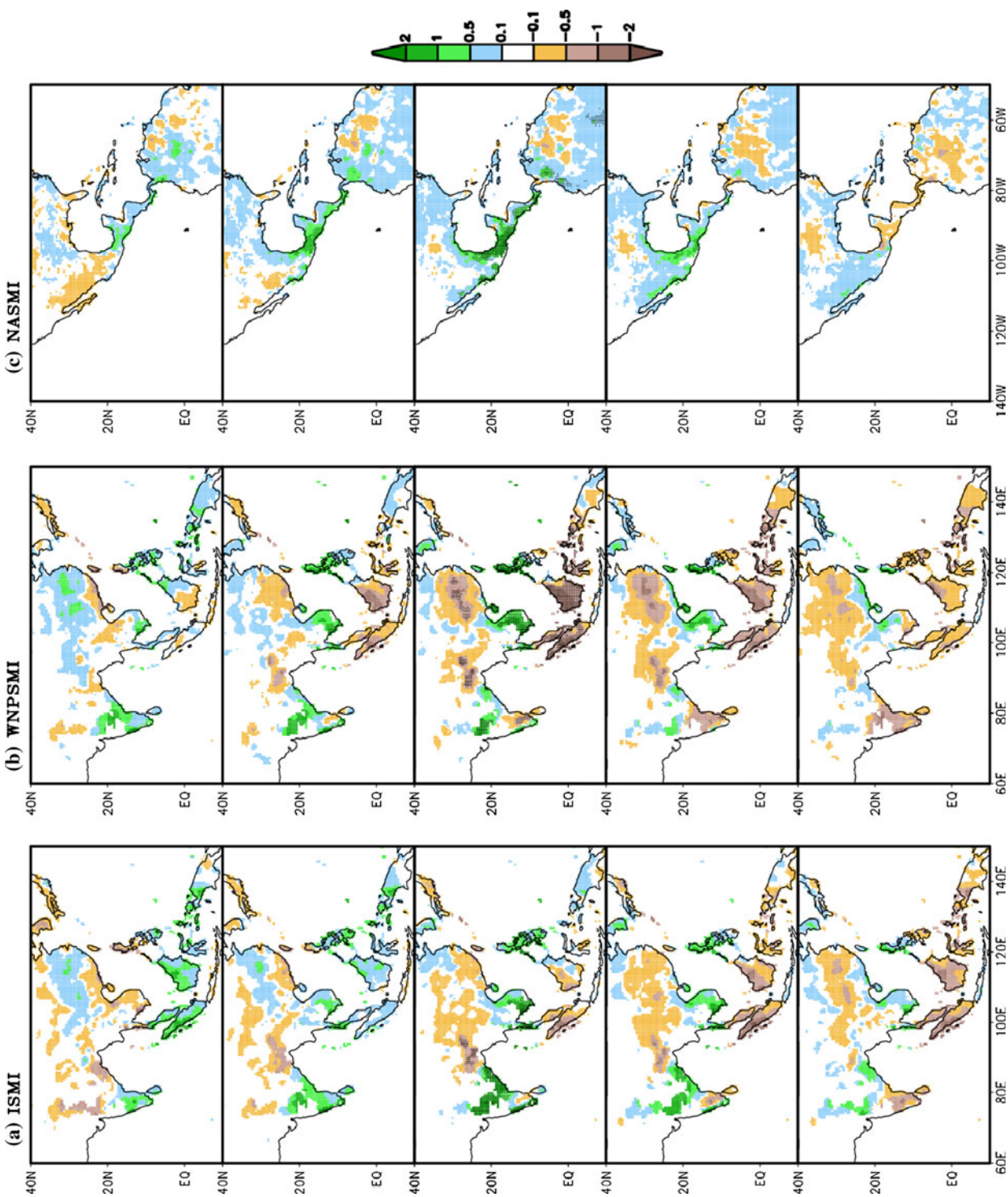

Fig. 7 Same as in Fig. 6 but for precipitation with reference to the **a** ISM, **b** WNPSM, and **c** NASM indices from −10 to +10 day with a 5-day time interval. The unit of precipitation is mm/day. *Shaded regions* indicate the precipitation that are statistically significant at above 95 % confidence level

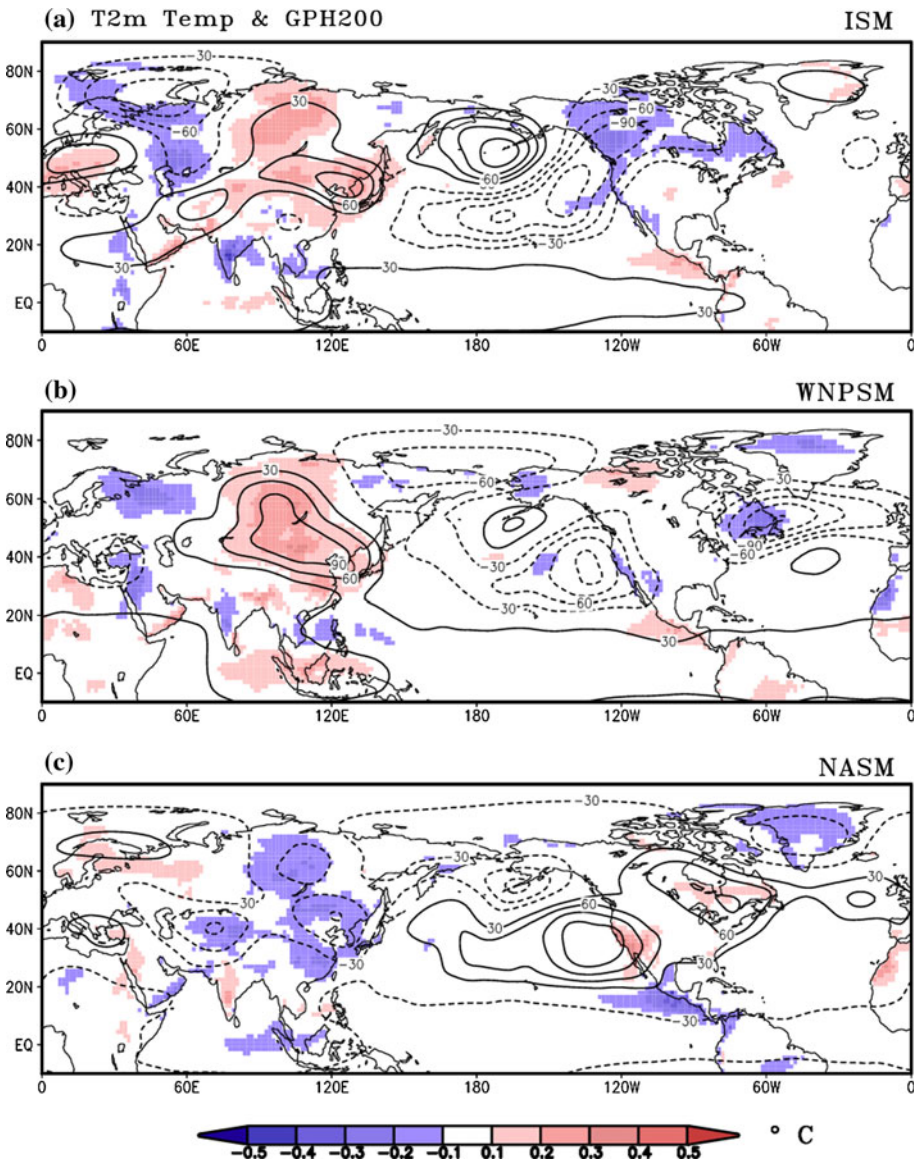

Fig. 8 The regressed intraseasonal anomalies of 2 m air temperature (T2m Temp, *shaded*) and GPH200 (*contour*) with reference to the **a** ISM, **b** WNPSM, and **c** NASM indices. The unit of T2m Temp and GPH200 are °C and gpm, respectively. *Shaded regions* indicate the T2m Temp that are statistically significant at above 95 % confidence level

which is consistent with the results of Jiang and Lau (2008) and other previous studies that had examined the rainfall/drought of the western or central US (Liu et al. 1998; Newman and Sardeshmukh 1998; Schubert et al. 2011). They showed the variations in WNP convection are correlated with the intraseasonal variability of the monsoons in both North America and East Asian/WNP sectors. It is also noteworthy that this relationship is found in 30–60 day time scale in our study while other studies focused on the time scale shorter than 30 day.

4.3 The teleconnection associated with the NASM ISO

Similar to the opposite anomaly patterns associated with the ISM and NASM ISO (Fig. 3), Fig. 6c shows that the time evolution of the convective anomalies associated with the NASM ISO also closely resemble the negative evolution patterns of Fig. 6a. It is of note that the convective activity over the eastern Pacific near Mexico evolves northward to southern US with increased amplitude on the western side from day −10 to +5 and decays from day +5.

In Fig. 6c, the teleconnection pattern shows opposite signal with Fig. 6a, but the convective activity is much strengthened near Mexico. From day −10 to 0, two anticyclonic anomalous centers over the southern North Pacific and western Canada propagate slowly eastward. When the eastward evolving meridional tripole approaches eastern Pacific, the anticyclonic center over the North Pacific is reinforced by the localized heating near Mexico during the active phase of NASM. From day 0 to +10, the arch-shaped downward energy transfer from the North Pacific to western coast of US along the jet can be detected.

5 Precipitation and temperature anomalies associated with BSISO teleconnection

In this section, we will discuss how the distributions of precipitation and surface air temperature intraseasonal anomalies are associated with BSISO teleconnection which will provide helpful information on intraseasonal prediction for the global NH monsoon domains.

Figure 7 shows the temporal evolution of the regressed precipitation associated with intraseasonal monsoon indices. Overall, the precipitation has positive anomalies along each monsoon domains corresponding to the evolution of the convective activity in Fig. 6. From India southeastward to Philippines, enhanced precipitation prevails in ISM and WNPSM active phase. To the north/south, the opposite tendency dominates from central to eastern China/Maritime Continent. Note that the meridional precipitation contrast is more compact and intensified in WNPSMI than ISMI. In Fig. 7c, there is large rainfall occurring over the southern Mexico at day −5, and then slowly evolves northward along the western and eastern coast of northern Mexico, and to southeastern US. It is interesting to find the opposite rainfall tendency in the northern part of South America with the Amazon basin.

The fractional variance within 10–40 % of intraseasonal rainfall explained by each monsoon indices mainly locate over the monsoon domains (not shown). Meanwhile, the 10–20 % of relatively high variance occur over the central/eastern China and the largest variance exist over the Maritime Continent in WNPSMI.

The 2 m air temperature and GPH200 distributions associated with each monsoon index at lag 0 is displayed in Fig. 8. It is evident that the negative temperature anomaly is emphasized at the maximum center of each monsoon domains, induced by the cooling from the rainfall over the area. The surface air temperature by all monsoon indices accord well with the geopotential height distribution over the extratropics, hence the tripole centers over central Russia, central Asia, East Asia show warmer tendency during ISM active phase while western Russia including West Asia, Canada, and western coast of US have cold temperature anomalies during the same phase. In Fig. 8b, the warm temperature anomaly is more enlarged over the Russia and Asia sector, while in Fig. 8c, the western US and eastern Canada have the higher warm temperature anomalies and cold air prevails over the Eurasian continent.

From Figs. 7 and 8, it is evident that the intraseasonal precipitation anomalies over the Eurasian and American continent evolve in phase with the BSISO evolution and the surface air temperature anomalies highly correspond to the evolution of the BSISO teleconnection.

6 Conclusion

The present study investigates the BSISO teleconnection associated with three intraseasonal monsoon activity centers and their time evolution features in the global perspective.

In the NH summer, there are three large convective intraseasonal variability centers along the 10°–20°N latitude bands over the Indian summer monsoon, Western North Pacific summer monsoon, and North American summer monsoon domains. In the tropics, zonally elongated band of active convection from Arabian Sea via India, Bay of Bengal, South China Sea, and Philippine Sea with light convective activity extending to the central Pacific prevail when the ISM activates. The active phase of WNPSM also forms as a band type with the signal over the Indian subcontinent—Bay of Bengal weakening, WNP more intensified, and the central tropical Pacific weakened. When the intraseasonal NASM activates, there is a seesaw convective teleconnection with the ISM active phase, showing the cohesive opposite signal.

Boreal summer intraseasonal oscillation teleconnections associated with three monsoon ISO centers showed some common quasi-stationary evolution as well as eastward evolution features. There are preferred teleconnection centers occurring over the NH continents: Europe, Russia, central Asia, East Asia, western US, and eastern US and Canada. Most of these regions are embedded in the waveguide along the jet stream, but the Europe and Russia centers are to the north of the waveguide, and eventually moved southward and merged within the waveguide. The intraseasonal variability over these locations can be largely modulated by the BSISO evolution and should be considered as important locations for intraseasonal prediction. The time evolution of the wave activity flux showed that at the exit of each waveguide of the jets, there is southeastward and northeastward split of the wave energy transfer: at the North African-Asian jet exit the wave energy transfer toward southeastward (northeastward) along the western coast of US (to Canada); and at the North Atlantic jet exit the energy propagates southeastward (northeastward) to the upstream of the North African jet (to Europe and Russia).

Boreal summer intraseasonal oscillation teleconnection not only had quasi-stationary but also the eastward evolutionary features evident over the Pacific-US sector, along with the eastward migration of the BSISO convection over the tropics. This has not been highlighted in the previous studies since the summer ISO includes complex evolutionary features, so as the teleconnection. The large scale of the north–south circulation anomalies along with the tropical convective activity can perturb the extratropical waves that span along the waveguides.

From the precipitation distribution according to three monsoon indices, central/eastern China, Maritime Continent, Mexico had significantly opposite tendency with the enhanced rainfall over the monsoon domains in Indo-western Pacific. The opposite tendency of the rainfall between northern South America and Amazon basin was also found. The BSISO teleconnection had significantly consistent pattern with the surface air temperature, except for the opposite tendency at the center of the monsoon domain which is induced by the cooling from the precipitation.

To better understand and explain the tropical influence on the extratropical circulation anomalies in the NH, further analysis will be needed with the numerical experiment to verify the results found in the present study. It is also important to extend our analysis to previous a few decades to see whether there is any interdecadal modulation of intraseasonal teleconnection over the globe.

Acknowledgments This work was supported by the Climate Dynamics Program of the National Science Foundation under award No AGS-1005599 and by GRL grant of the National Research Foundation (NRF) funded by Korean government (MEST) (No. 2011-0021927). ECMWF ERA-Interim data used in this study have been obtained from the ECMWF data server. This manuscript is SOEST Contribution No. 8677 and IPRC contribution No. 888.

References

Annamalai H, Slingo JM (2001) Active/break cycles: diagnosis of the intraseasonal variability of the Asian summer monsoon. Clim Dyn 18:85–102

Chen TC, Murakami M (1988) The 30–50 day variation of convective activity over the western Pacific Ocean with the emphasis on the northwestern region. Mon Weather Rev 116:892–906

Comeaux JL (1991) The origion and structure of the low-frequency modes. MS thesis Florida State University, Tallahassee, FL

Ding Q, Wang B (2007) Intraseasonal teleconnection between the summer Eurasian wave train and the Indian monsoon. J Clim 20:3751–3767

Duchon CE (1979) Lanczos filtering in one and two dimensions. J Appl Meteorol 18:1016–1022

Fukutomi Y, Yasunari T (1999) 10–25-day intraseasonal variations of convection and circulation over East Asia and western North Pacific during early summer. J Meteorol Soc Jpn 77:753–769

Higgins RW, Schemm JKE, Shi W, Leetmaa A (2000) Extreme precipitation events in the western United States related to tropical forcing. J Clim 13:793–820

Hsu HH, Weng CH, Wu CH (2004) Contrasting characteristics between the northward and eastward propagation of the intraseasonal oscillation during the boreal summer. J Clim 17:727–743

Jiang X, Lau NC (2008) Intraseasonal teleconnection between North American and western North Pacific monsoons with 20-day time scale. J Clim 21:2664–2679

Jiang X, Waliser DE (2009) Two dominant subseasonal variability modes of the eastern Pacific ITCZ. Geophys Res Lett 36:L04704. doi:10.1029/2008GL036820

Jiang X, Li T, Wang B (2004) Structures and mechanisms of the northward propagating boreal summer intraseasonal oscillation. J Clim 17:1022–1039

Kawamura R, Murakami T, Wang B (1996) Tropical and mid-latitude 45-day perturbations over the western Pacific during the northern summer. J Meteorol Soc Jpn 74:867–890

Kemball-Cook S, Wang B (2001) Equatorial waves and air-sea interaction in the boreal summer intraseasonal oscillation. J Clim 14:2923–2942

Kikuchi K, Wang B (2009) Global perspective of the quasi-biweekly oscillation. J Clim 22:1340–1359

Kikuchi K, Wang B (2010) Formation of tropical cyclones in the northern Indian Ocean associated with two types of tropical intraseasonal oscillation modes. J Meteorol Soc Jpn 88(3):475–496

Knutson TR, Weickmann KM, Kutzbach JE (1986) Global-scale intraseasonal oscillations of outgoing longwave radiation and 250 mb zonal wind during northern hemisphere summer. Mon Weather Rev 114:605–623

Krishnamurti TN, Sinha MC, Krishnamurti R, Oosterhof D, Comeaux J (1992) Angular momentum, length of day and monsoonal low frequency mode. J Meteorol Soc Jpn 70:131–166

Lee JY, Wang B, Kang IS, Shukla J et al (2010) How are seasonal prediction skills related to models' performance on mean state and annual cycle? Clim Dyn 35:267–283

Lee JY, Wang B, Ding Q, Ha KJ, Ahn JB, Kumar A, Stern B, Alves O (2011) How predictable is the northern hemisphere summer upper-tropospheric circulation? Clim Dyn 37:1189–1203

Liu AZ, Ting M, Wang H (1998) Maintenance of circulation anomalies during the 1988 drought and 1993 floods over the United States. J Atmos Sci 55:2810–2832

Lorenz DJ, Hartmann DL (2006) The effect of the MJO on the North American monsoon. J Clim 19:333–343

Madden RA, Julien PR (1971) Detection of a 40–50 day oscillation in the zonal wind in the tropical Pacific. J Atmos Sci 28:702–708

Mao JY, Chan JCL (2005) Intraseasonal variability of the South China Sea summer monsoon. J Clim 18:2388–2402

Mo KC (2000) Intraseasonal modulation of summer precipitation over North America. Mon Weather Rev 128:1490–1505

Mullen SL, Schmitz JT, Renno NO (1998) Intraseasonal variability of the summer monsoon over southeast Arizona. Mon Weather Rev 126:3016–3035

Newman M, Sardeshmukh PD (1998) The impact of the annual cycle on the North Pacific/North American response to remote low-frequency forcing. J Atmos Sci 55:1336–1353

Plumb RA (1985) On the three-dimensional propagation of stationary waves. J Atmos Sci 42:217–229

Schubert S, Wang H, Suarez M (2011) Warm season subseasonal variability and climate extremes in the Northern Hemisphere: the role of stationary Rossby waves. J Clim 24:4773–4792

Teng H, Wang B (2003) Interannual variations of the boreal summer intraseasonal oscillation in the Asia-Pacific region. J Clim 16:3572–3584

Wang B, Fan Z (1999) Choice of South Asian summer monsoon indices. Bull Am Meteorol Soc 80:629–638

Wang B, Rui H (1990) Synoptic climatology of transient tropical intraseasonal convection anomalies: 1975–1985. Meteorol Atmos Phys 44:43–61

Wang B, Xie X (1997) A model for the boreal summer intraseasonal oscillation. J Atmos Sci 54:72–86

Wang B, Wu RG, Lau KM (2001) Interannual variability of the Asian summer monsoon: contrasts between the Indian and the western North Pacific-east Asian monsoon. J Clim 14:4073–4090

Wang B, Webster B, Kikuchi K, Yasunari T, Qi Y (2006) Boreal summer quasi-monthly oscillation in the global tropics. Clim Dyn 27:661–675

Wang B, Lee JY, Shukla J, Kang IS et al (2009) Advance and prospectus of seasonal prediction: assessment of APCC/CliPAS 14-model ensemble retrospective seasonal prediction (1980–2004). Clim Dyn 33:93–117

Xie P, Yatagai A, Chen M, Hayasaka T, Fukushima Y, Liu C, Yang S (2007) A gauge-based analysis of daily precipitation over East Asia. J Hydrometeorol 8:607–626

Yang J, Wang B, Wang B (2008) Anticorrelated intensity change of the quasi-biweekly and 30–50-day oscillations over the South China Sea. Geophys Res Lett 35:L16702. doi:10.1029/2008GL034449

Yasunari T (1979) Cloudiness fluctuations associated with the Northern Hemisphere summer monsoon. J Meteorol Soc Jpn 57:227–242

Zhu B, Wang B (1993) The 30–60 day convection seesaw between the tropical Indian and western Pacific Oceans. J Atmos Sci 50:184–199